Inertial interaction in pile-groups: a study of the influence of coupling via an iterative wave-scattering approach

T.L. Edirisinghe (tle25@cam.ac.uk), J.P. Talbot

University of Cambridge, Department of Engineering, Cambridge, CB2 1PZ, United Kingdom

---

Abstract

The increasing urban population is leading to the exploitation of building sites close to sources of ground-borne vibration, such as railways and busy roads. Piled foundations can provide a significant vibration transmission path into a building, which can then cause disturbance to occupants and sensitive equipment. There is a strong need to develop numerical models that can capture the essential dynamics of a piled foundation, over the frequency range associated with ground-borne vibration, to help practising engineers decide on appropriate countermeasures. In this paper, a piled foundation is modelled as a pile-group embedded in a homogeneous half-space. Previous research has explored the dynamics of pile groups to inertial loading at relatively low frequencies, over the seismic range. Here, an iterative approach is developed using a source-receiver boundary-element model to account for the wave-scattering effect that becomes more significant at higher frequencies. Predictions of the dynamic interaction factors, which describe the pile-soil-pile interaction, show very good agreement with a standard boundary-element model for a range of geometric and material parameters. The results show that using uncoupled source-receiver models can account effectively for the interaction between piles without resorting to fully coupled models, even at frequencies well above those of previously published results.

Keywords: Ground-borne vibration, Pile-group dynamics, Inertial loading, Soil-structure interaction, Wave scattering, Dynamic interaction factors

---

1. Introduction

An understanding of the dynamics of piled foundations is essential for the seismic assessment of many buildings. It is also essential for the serviceability assessment of buildings subjected to ground-borne vibration, from sources such as railways and busy roads [1]. In such cases, piles can provide a significant vibration transmission path, both into and out of the building, and this must be accounted for in any assessment of the likely internal vibration levels. The frequencies of interest extend well beyond the seismic range, up to as high as 250 Hz in some cases, and the associated wavelengths are now comparable with the dimensions of a typical foundation. Wave-scattering effects are therefore more significant, and theoretical models developed purely for seismic analysis can be of limited use.

1.1. Existing pile-group models

The dynamics of pile groups, in which multiple piles are connected to a common pile-cap supporting the superstructure, can be categorised according to the mode of excitation: so-called, inertial and kinematic loading. This study focuses on the former, in which the piles within a group respond to forces and moments applied at the pile-head of one or more piles. Our particular interest lies in the soil-structure interaction that occurs between nearby piles, known as pile-soil-pile interaction (PSPI).

There is extensive literature available on the modelling of piled foundations; a thorough review is presented by Kuo and Hunt [2]. When the spacing between piles in a group is small, it is known that PSPI needs to be accounted for when modelling the group's dynamic response. There are two important effects. Soil stiffening dominates under static and low-frequency loading, when the wavelengths in the soil are greater than the pile spacing, and this occurs within the vicinity of the pressure bulb surrounding each excited pile, where the soil stresses (and strains) are significant. At higher frequencies, wave-scattering effects become significant as the wavelengths in the soil approach the length scale of the pile diameter. Dynamic interaction factors are commonly used to characterise PSPI. These are calculated for any pair of neighbouring piles within a group by ignoring the presence of nearby piles; the dynamic stiffness of the overall pile-group is then obtained through the superposition of appropriate interaction factors.

Semi-analytical models developed by Dobry, Gazetas and Makris [3]–[6] are some of the first to calculate frequency-dependent interaction factors, by representing a pair of piles as an uncoupled source-receiver system. The source sub-system models the excited pile to calculate the response of the surrounding soil in the absence of the second pile (the receiver). The wave-field that propagates away from the source, assuming the receiver does not influence the field, is applied as an incident excitation on the receiver sub-system. However, this approach is less accurate at high frequencies when the receiver can scatter the incident waves, which, in turn, can propagate back to excite the source. Furthermore, when the piles are close together, the receiver can influence the wave-field propagating away from the source, and this can occur even at low frequencies if the pressure bulb around the source also encompasses the receiver. Both of these effects can lead to inaccuracies in the uncoupled source-receiver model.

The alternative approach is to model the full pile-group as a coupled system, which directly accounts for the PSPI. Kaynia and Kausel [7], [8] derived matrix equations for the dynamic response of a pile-group and produced a model based on a rigorous boundary-element method (BEM) formulation. Generally good agreement is observed between this model and uncoupled source-receiver models, and the agreement improves as the pile spacing increases. However, the results are presented over non-dimensional frequencies that do not extend to the high-frequency content of ground-borne vibration. Another concern is that the soil's flexibility matrix is computed by superposing a 'fictitious' column onto the soil at the location of each pile, such that the flexural and inertial properties of the composite solid (i.e. the column and soil) are equivalent to the pile [7]. The pile cavity in the soil is therefore not represented, and this can lead to inaccuracies in the results at high frequencies, as concluded by Mamoon et al. [9].

The aim of this paper is to investigate if the use of interaction factors, for vertical, lateral and rotational motion at the pile-heads of a generic pile-group, accounts effectively for PSPI over a range of non-dimensional frequencies a_0, which correspond to ground-borne vibration in London

Clay in the range $1 - 160$ Hz. A set of non-dimensional graphs is presented that plot interaction factors as functions of frequency, to investigate how a typical range of fundamental material and geometric parameters influence PSPI. Two methods of modelling a pile-group are presented:

1. a direct method is used to model a pile-group as a coupled system, with all pile cavities explicitly included in the soil;

2. an indirect method is used to model a pile-group as a source-receiver system by dividing it into two isolated sub-systems, representing the source and receiver, which are then coupled together using an iterative wave-scattering approach.

The direct method is used to investigate the influence of neighbouring and intermediate piles on the interaction factors, whilst the indirect method is explored as an alternative means of accounting for the PSPI between multiple soil-embedded structures.

1.2. The iterative wave-scattering approach

There are a variety of techniques used to solve problems where waves interact with multiple neighbouring obstacles in a medium [10]. An iterative approach can be used to dynamically couple all the obstacles in the system by treating each obstacle as an isolated sub-system and accounting for waves that propagate back-and-forth between them.

As previously stated, the uncoupled source-receiver approach accounts only for the initial 'outgoing' wave-field from the source that interacts with the receiver; this is equivalent to the first iteration in the iterative approach. In the second iteration, the 'incoming' wave-field that propagates back towards the source, due to the scattered field at the receiver, is calculated. The motion of the source, due to both the pile-head load and the incident field from the receiver, causes another incident field to propagate towards the receiver, which gives a revised solution for the response of the two piles compared to the first iteration. During each iteration, the source and receiver sub-systems are therefore weakly coupled. When this process is repeated for multiple iterations, the response converges to the solution for when the source and receiver are fully coupled. An advantage of the approach is that it provides additional insight into the wave-scattering behaviour, compared to a coupled system: if multiple iterations are required to converge to the coupled solution, then the wave-scattering effect is clearly more significant than if only one iteration is required. It is worth noting that the approach does not offer significant computational advantages over the direct method (the element meshes are comparable and more memory is required to manage the iterations).

The iterative approach has been used to analyse wave-scattering problems in electromagnetism [11], [12], acoustics [13] and elastodynamics [14], [15]. Ongoing research is investigating an iterative approach to predict the soil response around underground railway tunnels [16].

2. Modelling

This section presents the single-pile model that provides the fundamental unit for coupling N piles together in a generalised pile-group, using either the direct or indirect methods. The applied loads are assumed to be time-harmonic, with the models formulated in the space-frequency $(\mathbf{x}, \omega)$-domain, where $\mathbf{x}$ is a position vector and ω is the excitation angular frequency. For example, the displacement response vector $\bar{\mathbf{u}}$ in the space-time $(\mathbf{x}, t)$-domain is given by

$$\bar{\mathbf{u}}(\mathbf{x}, t) = \mathrm{Re}\left(\mathbf{u}(\mathbf{x}, \omega) e^{i\omega t}\right) \tag{1}$$

where $\mathbf{u}$ a vector of complex $(i = \sqrt{-1})$ amplitudes in the $(\mathbf{x}, \omega)$-domain. For clarity, the exponential term is omitted from the remainder of the paper. Linear behaviour is assumed because of the low strain amplitudes associated with ground-borne vibration [17].

2.1. Modelling the soil

In common with much of the previous work on pile dynamics, the soil domain in this study is modelled using the BEM [8], [18]–[20]. Since no artificial boundaries are imposed, this method accounts properly for the semi-infinite nature of the domain, avoiding spurious reflections and ensuring that radiation damping is inherently accounted for. The BEM models used here incorporate the Green's functions for a homogeneous, isotropic full-space, of mass density ρ_s, Poisson's ratio ν_s, shear modulus G_s and hysteric loss factor η_s. This accounts for the essential dynamic behaviour of the soil, although alternative Green's functions may be employed if necessary, such as those for layered soil. Constant boundary elements are used, so the field variables are assumed to be uniform over each element.

The three-dimensional, half-space domain of the soil is defined by two boundaries: the free surface and the soil-pile interface, which defines the cavity into which the pile model is coupled. Square elements are used for both boundaries, and the pile cross-section is assumed to be square. By comparing more refined BEM models, the latter has been found to offer a good compromise between accuracy and computational efficiency [19], [20]. Further convergence studies at higher frequencies ($a_0 = 3.2$), which consider the pile-head compliance of a single pile with increasingly circular cross-sections (4-element square, 8-element octagonal and 16-element sections), support this choice. The mesh consists of N_{T} elements in total. The minimum numbers of elements N_1 and N_2 that form the edges of the free surface are found by increasing these until convergence is achieved in the particular response of interest. For a group of N piles, the free surface and soil-pile interface comprise $N_{\mathrm{FS}} = N_1 N_2 - N$ and $N_{\mathrm{SP}} = \sum_{k=1}^{N} n_{\mathrm{SP}}^{(k)}$ elements, where $n_{\mathrm{SP}}^{(k)}$ is the number of elements associated with pile k. The mesh density is varied depending on the frequency, so that at least six elements per shear wavelength are used, as recommended by Domínguez [21]. For the material properties adopted here, the elements have side-length $b = 0.5\ \mathrm{m}$ for frequencies below 80 Hz, while at higher frequencies $b = 0.25\ \mathrm{m}$.

The field variables are defined by two vectors that give the complex amplitudes of the displacement and traction fields evaluated at the central node of each element. The displacement field $\mathbf{u}$ in the Cartesian x, y, z directions is defined as

$$\mathbf{u} = \left\{ {u_x}^1, {u_y}^1, {u_z}^1 \mid {u_x}^2, {u_y}^2, {u_z}^2 \mid \ \ldots \ \mid {u_x}^{N_{\mathrm{T}}}, {u_y}^{N_{\mathrm{T}}}, {u_z}^{N_{\mathrm{T}}} \right\}^{\mathrm{T}} \tag{2}$$

where $\mathbf{u}^j = \left\{ {u_x}^j, {u_y}^j, {u_z}^j \right\}^{\mathrm{T}}$ is the displacement vector at node j and the superscript T denotes the vector transpose, with the traction field $\mathbf{p}$ defined similarly. The BEM relationship between the field variables is then

$$\mathbf{Hu} = \mathbf{Gp} \tag{3}$$

where $\mathbf{H}$ and $\mathbf{G}$ are the frequency-dependent collocation matrices, which are assembled using the formulation described by Domínguez [21].

Equation (3) can be rearranged as

$$\mathbf{u} = \mathbf{H}^{-1}\mathbf{G}\mathbf{p} = \mathbf{H}_{\mathrm{S}}\mathbf{p} \tag{4}$$

and $\mathbf{H}_{\mathrm{S}}$, the resulting displacement frequency-response function (FRF) matrix of the soil, can be partitioned into sub-matrices:

$$\begin{Bmatrix} \mathbf{u}_{\mathrm{FS}} \\ \mathbf{u}_{\mathrm{SP}}^{1} \\ \mathbf{u}_{\mathrm{SP}}^{2} \\ \vdots \\ \mathbf{u}_{\mathrm{SP}}^{N} \end{Bmatrix} = \begin{bmatrix} \mathbf{H}_{\mathrm{S11}} & \mathbf{H}_{\mathrm{S12}} \\ \mathbf{H}_{\mathrm{S21}} & \mathbf{H}_{\mathrm{S22}} \end{bmatrix} \begin{Bmatrix} \mathbf{p}_{\mathrm{FS}} \\ \mathbf{p}_{\mathrm{SP}}^{1} \\ \mathbf{p}_{\mathrm{SP}}^{2} \\ \vdots \\ \mathbf{p}_{\mathrm{SP}}^{N} \end{Bmatrix} \tag{5}$$

$$\mathbf{u}_{\mathrm{FS}} = \mathbf{H}_{\mathrm{S11}}\mathbf{p}_{\mathrm{FS}} + \mathbf{H}_{\mathrm{S12}}\mathbf{p}_{\mathrm{SP}} \tag{6}$$

$$\mathbf{u}_{\mathrm{SP}} = \mathbf{H}_{\mathrm{S21}}\mathbf{p}_{\mathrm{FS}} + \mathbf{H}_{\mathrm{S22}}\mathbf{p}_{\mathrm{SP}} \tag{7}$$

where the subscripts FS and SP denote the field variables at the free surface and soil-pile interface, with $\mathbf{u}_{\mathrm{SP}} = \left\{\mathbf{u}_{\mathrm{SP}}^{1}, \mathbf{u}_{\mathrm{SP}}^{2}, \ldots, \mathbf{u}_{\mathrm{SP}}^{N}\right\}^{\mathrm{T}}$ and $\mathbf{p}_{\mathrm{SP}} = \left\{\mathbf{p}_{\mathrm{SP}}^{1}, \mathbf{p}_{\mathrm{SP}}^{2}, \ldots, \mathbf{p}_{\mathrm{SP}}^{N}\right\}^{\mathrm{T}}$.

Eqs. (6) and (7) can only be used to calculate the displacement and traction fields at the boundaries of the soil domain. Whilst this is suitable for coupling the pile model, a variation of the integral formulation is required to find the field variables at internal points within the domain. Domínguez [21] describes the process of finding the displacements at internal points, but not the tractions. The latter are derived in Appendix A from the integral form of the displacements, using the same notation as Domínguez. From there, Eq. (A.12) can be expressed in matrix form to give the vector of displacements at selected internal points:

$$\mathbf{u}^{\mathrm{int}} = \mathbf{G}_{u}\mathbf{p} - \mathbf{H}_{u}\mathbf{u} \tag{8}$$

where $\mathbf{G}_u$ and $\mathbf{H}_u$ are the displacement-state matrices.

Similarly, Eq. (A.13) can be expressed to give the corresponding vector of tractions:

$$\mathbf{p}^{\text{int}} = \mathbf{G}_p \mathbf{p} - \mathbf{H}_p \mathbf{u} \tag{9}$$

where $\mathbf{G}_p$ and $\mathbf{H}_p$ are the traction-state matrices.

By substituting the field variables at the boundaries of the soil domain, as expressed in Eqs. (6) and (7), into Eqs. (8) and (9), the final expressions for the internal displacements and tractions are:

$$\mathbf{u}^{\text{int}} = \mathbf{G}_u \begin{Bmatrix} \mathbf{p}_{\text{FS}} \\ \mathbf{p}_{\text{SP}} \end{Bmatrix} - \mathbf{H}_u \begin{Bmatrix} \mathbf{u}_{\text{FS}} \\ \mathbf{u}_{\text{SP}} \end{Bmatrix} \tag{10}$$

$$\mathbf{p}^{\text{int}} = \mathbf{G}_p \begin{Bmatrix} \mathbf{p}_{\text{FS}} \\ \mathbf{p}_{\text{SP}} \end{Bmatrix} - \mathbf{H}_p \begin{Bmatrix} \mathbf{u}_{\text{FS}} \\ \mathbf{u}_{\text{SP}} \end{Bmatrix}. \tag{11}$$

2.2. Modelling the pile

The pile model uses the analytical solutions for an elastic bar and Euler-Bernoulli beam to describe the longitudinal and transverse motion of a three-dimensional pile, as adopted by Talbot and Hunt [19]. The model is characterised by its length L, mass density ρ_p, diameter d, Young's modulus E_p and second moment of inertia I_p. Material damping in the pile is neglected because its response is dominated by radiation damping in the soil, although this can be easily included by specifying a complex Young's modulus. The effects of rotational inertia and shear deformation are also neglected, the errors introduced by Euler's assumptions being minimal at the frequencies associated with ground-borne vibration. Loading may be applied at the pile-head as a combination of forces and moments, although torsion about the longitudinal (vertical) axis is ignored.

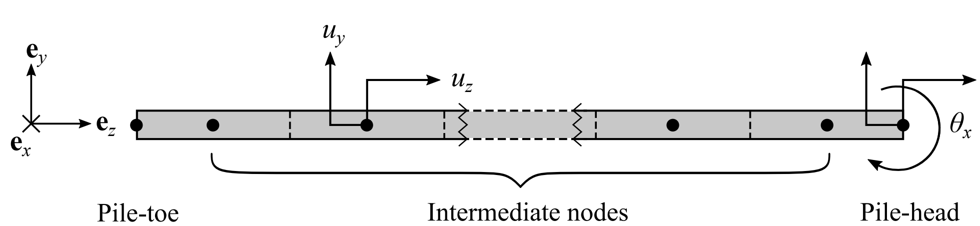

Figure 1: The pile model, based on the solutions for an elastic bar and Euler-Bernoulli beam (drawn horizontally in the (y, z)-plane). The dots represent the nodes for coupling to the boundary elements of the soil-pile interface.

To enable coupling to the soil, equally-spaced intermediate nodes are defined along the pile's centroidal axis, with a further two nodes at the pile head and toe, as shown in Fig. 1. By considering unit forces at each node, and the additional application of a unit moment at the pile-head node, the displacement FRF matrix $\mathbf{H}_{\mathrm{P}}^{(k)}$ for pile k can be computed. This is then partitioned into sub-matrices:

$$\begin{Bmatrix} \mathbf{u}_{\mathrm{PH}}^{(k)} \\ \mathbf{u}_{\mathrm{P}}^{(k)} \end{Bmatrix} = \begin{bmatrix} \mathbf{H}_{\mathrm{P11}}^{(k)} & \mathbf{H}_{\mathrm{P12}}^{(k)} \\ \mathbf{H}_{\mathrm{P21}}^{(k)} & \mathbf{H}_{\mathrm{P22}}^{(k)} \end{bmatrix} \begin{Bmatrix} \mathbf{f}_{\mathrm{PH}}^{(k)} \\ \mathbf{f}_{\mathrm{P}}^{(k)} \end{Bmatrix} \tag{12}$$

where the subscripts PH and P denote variables at the pile head and intermediate nodes respectively. Expanding the first and second rows of Eq. (12) gives:

$$\mathbf{u}_{\mathrm{PH}}^{(k)} = \mathbf{H}_{\mathrm{P11}}^{(k)}\mathbf{f}_{\mathrm{PH}}^{(k)} + \mathbf{H}_{\mathrm{P12}}^{(k)}\mathbf{f}_{\mathrm{P}}^{(k)} \tag{13}$$

$$\mathbf{u}_{\mathrm{P}}^{(k)} = \mathbf{H}_{\mathrm{P21}}^{(k)}\mathbf{f}_{\mathrm{PH}}^{(k)} + \mathbf{H}_{\mathrm{P22}}^{(k)}\mathbf{f}_{\mathrm{P}}^{(k)}\,. \tag{14}$$

Note that, unlike $\mathbf{H}_{\mathrm{S}}$, $\mathbf{H}_{\mathrm{P}}^{(k)}$ relates displacements and forces, rather than tractions.

Finally, consider the coupling conditions between the soil and a pile. The pile is assumed to be perfectly bonded to the soil, which is justified given the low amplitudes of ground-borne vibration. Each pile node, with the exception of that at the pile head, is therefore coupled directly to the surrounding nodes of the four boundary elements representing the soil–pile interface. Thus, satisfying compatibility and equilibrium at the soil-pile interface requires

$$\mathbf{u}_{\mathrm{SP}}^{(k)} = \mathbf{Q}_1^{(k)}\mathbf{u}_{\mathrm{P}}^{(k)} \tag{15}$$

and

$$\mathbf{f}_{\mathrm{P}}^{(k)} = -b^2{\mathbf{Q}_1^{(k)}}^{\mathrm{T}}\mathbf{p}_{\mathrm{SP}}^{(k)} = -\mathbf{Q}_2^{(k)}\mathbf{p}_{\mathrm{SP}}^{(k)} \tag{16}$$

where $\mathbf{Q}_1^{(k)}$ is a transformation matrix assembled from 3×3 identity matrices [19].

3. Calculation of Pile-Group Response

This section describes the calculation of the inertial response of a general pile-group containing N piles, when excited at the head of one of the piles. Details are provided for both the direct and indirect methods, using the models described in Section 2.

3.1. The direct method

By generalising Eq. (13) for N piles, the pile-head displacements at all piles in the group are given by

$$\mathbf{u}_{\mathrm{PH}} = \mathbf{H}_{\mathrm{P11}}\mathbf{f}_{\mathrm{PH}} + \mathbf{H}_{\mathrm{P12}}\mathbf{f}_{\mathrm{P}} \tag{17}$$

where $\mathbf{H}_{\mathrm{P11}}$ and $\mathbf{H}_{\mathrm{P12}}$ are global block-diagonal matrices that contain the sub-matrices $\mathbf{H}_{\mathrm{P11}}^{(k)}$ and $\mathbf{H}_{\mathrm{P12}}^{(k)}$, respectively, for each pile k along the leading diagonal, as defined in Appendix B. The global displacement and force vectors for the pile-group are represented by $\mathbf{u}_{\mathrm{PH}}$, $\mathbf{f}_{\mathrm{PH}}$ and $\mathbf{f}_{\mathrm{P}}$. Similar matrix expressions can be obtained by generalising Eqs. (14)–(16):

$$\mathbf{u}_{\mathrm{P}} = \mathbf{H}_{\mathrm{P21}}\mathbf{f}_{\mathrm{PH}} + \mathbf{H}_{\mathrm{P22}}\mathbf{f}_{\mathrm{P}} \tag{18}$$

$$\mathbf{u}_{\mathrm{SP}} = \mathbf{Q}_1\mathbf{u}_{\mathrm{P}} \tag{19}$$

$$\mathbf{f}_{\mathrm{P}} = \mathbf{Q}_2\mathbf{p}_{\mathrm{SP}} \tag{20}$$

where $\mathbf{H}_{\mathrm{P21}}$, $\mathbf{H}_{\mathrm{P22}}$, $\mathbf{Q}_1$ and $\mathbf{Q}_2$ are global block-diagonal matrices, also defined in Appendix B.

The governing equations for the pile-group, Eqs. (17)–(20), and the soil, Eqs. (7) and (8), are rearranged to get an expression for the tractions at the soil-pile interface $\mathbf{p}_{\mathrm{SP}}$ as a function of the applied pile-head load $\mathbf{f}_{\mathrm{PH}}$:

$$\mathbf{p}_{\mathrm{SP}} = \mathbf{A}\mathbf{Q}_1\mathbf{H}_{\mathrm{P21}}\mathbf{f}_{\mathrm{PH}} \tag{21}$$

where

$$\mathbf{A} = \left(\mathbf{H}_{\mathrm{S22}} + \mathbf{Q}_1\mathbf{H}_{\mathrm{P22}}\mathbf{Q}_2\right)^{-1}. \tag{22}$$

Note that a traction-free boundary condition is applied at the free surface ($\mathbf{p}_{\mathrm{FS}} = \mathbf{0}$) because this study is only concerned with pile-head excitation. By substituting Eq. (21) back into Eqs. (7), (8) and (17)–(20), the other field variables can be found.

3.2. The indirect method

The pile-group is divided into two sub-systems: the excited pile is referred to as the source, while all other piles in the group are collectively referred to as the receiver. Each iteration i of the method involves calculating the incident fields at the soil-pile interface of the receiver, when the source is excited, and vice-versa when the receiver is excited. Figure 2 illustrates the case for the displacement fields at the source $\left(\mathbf{u}_{\mathrm{SP}}^{S,\mathrm{inc}}\right)^i$ and receiver $\left(\mathbf{u}_{\mathrm{SP}}^{R,\mathrm{inc}}\right)^i$. The same approach is applied to compute the incident traction fields $\left(\mathbf{p}_{\mathrm{SP}}^{S,\mathrm{inc}}\right)^i$ and $\left(\mathbf{p}_{\mathrm{SP}}^{R,\mathrm{inc}}\right)^i$.

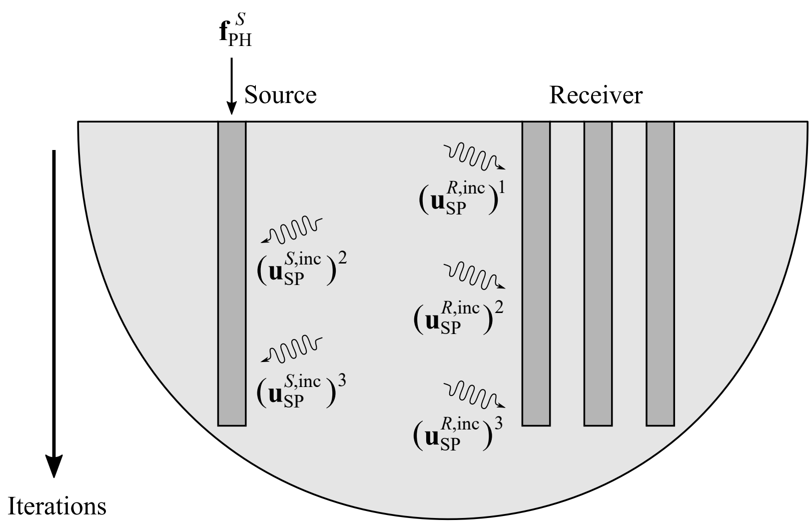

Figure 2: Schematic diagram illustrating the implementation of the indirect method for a pile-group containing four piles using three iterations. The pile-group is divided into two sub-systems: source and receiver.

Fig. 3 illustrates the BEM meshes used for the soil boundaries in both the direct and indirect methods. The BEM mesh for the source sub-system contains N_{FS}^S free surface elements and N_{SP}^S soil-pile interface elements. Similarly, the BEM mesh for the receiver sub-system contains N_{FS}^R and N_{SP}^S elements for the free surface and soil-pile interface. The receiver sub-system may consist of one or more piles, as illustrated in Figs. 2 and 3, where all the piles in the receiver are coupled

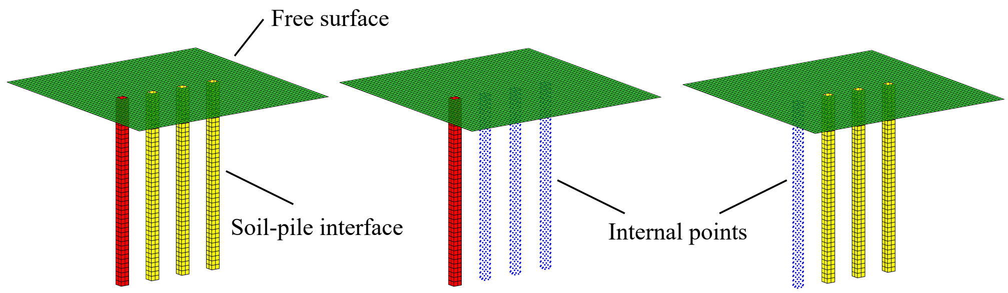

(a) Complete pile-group (b) Source sub-system (c) Receiver sub-system

Figure 3: The pile-group in Fig. 2 is modelled using three BEM meshes: (a) the complete pile-group, using the direct method; and (b) the source and (c) receiver sub-systems of the indirect method. Coloured elements represent the free surface (green) and the soil-pile interfaces for the source (red) and receiver (yellow). Internal points within the respective sub-systems are represented by blue dots.

together at their respective soil-pile interfaces. Note that the free surface in the source and receiver meshes is discretised to the same extent.

The following two sections derive the incident fields at the receiver and source, for each iteration, so that the two sub-systems can be weakly coupled together. For clarity, the superscript i, denoting the field variables for each iteration, is omitted.

3.2.1. The source sub-system

This section derives the scattered (radiated) fields induced at the source when this is excited in isolation, and then derives the incident fields that arrive, as a consequence, at the soil-pile interface of the receiver. Figure 4 illustrates the BEM meshes used for the source sub-system in a pile-group containing two piles, where mesh 1 is used to excite the source (pile 1) and mesh 2 is used to find the incident fields at the soil-pile interface of the receiver (pile 2). The free surface and soil-pile interface of pile 1 is discretised in both meshes, while mesh 2 also defines the soil-pile interface of pile 2 as a group of internal points within the unbounded domain of the source sub-system.

By applying the superposition principle, the total displacement field at the soil-pile interface of pile 1 $\mathbf{u}_{\mathrm{SP}}^{1}$ can be decomposed into a scattered field $\mathbf{u}_{\mathrm{SP}}^{1,\mathrm{sca}}$ and an incident field $\mathbf{u}_{\mathrm{SP}}^{1,\mathrm{inc}}$ component, such that $\mathbf{u}_{\mathrm{SP}}^{1} = \mathbf{u}_{\mathrm{SP}}^{1,\mathrm{sca}} + \mathbf{u}_{\mathrm{SP}}^{1,\mathrm{inc}}$. Similarly, for the total traction field: $\mathbf{p}_{\mathrm{SP}}^{1} = \mathbf{p}_{\mathrm{SP}}^{1,\mathrm{sca}} + \mathbf{p}_{\mathrm{SP}}^{1,\mathrm{inc}}$.

When the BEM is applied using mesh 1, the soil displacement FRF matrix $\mathbf{H}_{\mathrm{S}}^{1}$ of pile 1 can be

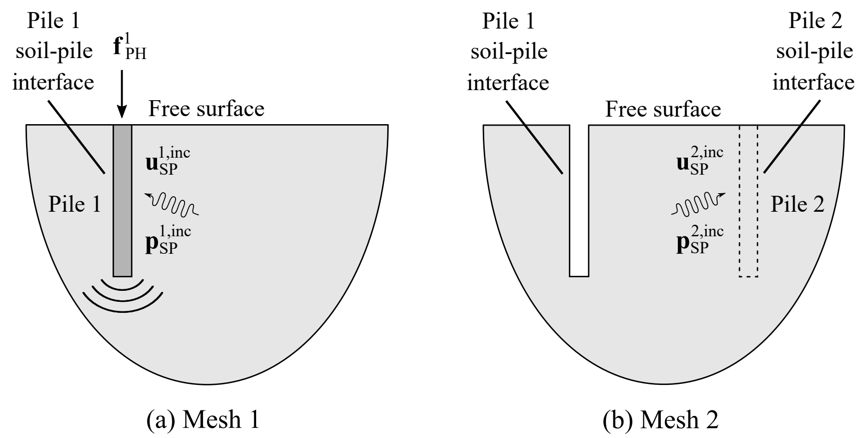

Figure 4: Schematic diagram illustrating the BEM meshes used for the unbounded domain of the isolated source subsystem in a pile-group containing two piles. Internal points within the source's domain lie along the dashed line in mesh 2. The darker and lighter shaded regions represent material of the pile and soil.

expressed in terms of the scattered fields at the mesh boundaries:

$$\left\{ \begin{matrix} \mathbf{u}^1_{\mathrm{FS}} \\ \mathbf{u}^1_{\mathrm{SP}} - \mathbf{u}^{1,\mathrm{inc}}_{\mathrm{SP}} \end{matrix} \right\} = \mathbf{H}^1_{\mathrm{S}} \left\{ \begin{matrix} \mathbf{p}^1_{\mathrm{FS}} \\ \mathbf{p}^1_{\mathrm{SP}} - \mathbf{p}^{1,\mathrm{inc}}_{\mathrm{SP}} \end{matrix} \right\} \tag{23}$$

where $\mathbf{u}^1_{\mathrm{FS}}$ and $\mathbf{p}^1_{\mathrm{FS}} = \mathbf{0}$ denote the displacement field and traction-free boundary condition at the free surface of pile 1. There are no (artificial) incident fields at the free surface because this is discretised to the same extent in both meshes. The $\mathbf{H}^1_{\mathrm{S}}$ matrix can be partitioned into sub-matrices:

$$\left\{ \begin{matrix} \mathbf{u}^1_{\mathrm{FS}} \\ \mathbf{u}^1_{\mathrm{SP}} - \mathbf{u}^{1,\mathrm{inc}}_{\mathrm{SP}} \end{matrix} \right\} = \begin{bmatrix} \mathbf{H}^1_{\mathrm{S11}} & \mathbf{H}^1_{\mathrm{S12}} \\ \mathbf{H}^1_{\mathrm{S21}} & \mathbf{H}^1_{\mathrm{S22}} \end{bmatrix} \left\{ \begin{matrix} \mathbf{0} \\ \mathbf{p}^1_{\mathrm{SP}} - \mathbf{p}^{1,\mathrm{inc}}_{\mathrm{SP}} \end{matrix} \right\}. \tag{24}$$

Since pile 1 represents the source, the superscript '1' can be replaced by S to denote this. The rows in Eq. (24) can then be expanded into two governing equations for the soil of the isolated source:

$$\mathbf{u}^S_{\mathrm{FS}} = \mathbf{H}^S_{\mathrm{S12}} \left(\mathbf{p}^S_{\mathrm{SP}} - \mathbf{p}^{S,\mathrm{inc}}_{\mathrm{SP}} \right) \tag{25}$$

$$\mathbf{u}^S_{\mathrm{SP}} - \mathbf{u}^{S,\mathrm{inc}}_{\mathrm{SP}} = \mathbf{H}^S_{\mathrm{S22}} \left(\mathbf{p}^S_{\mathrm{SP}} - \mathbf{p}^{S,\mathrm{inc}}_{\mathrm{SP}} \right) \tag{26}$$

Rearranging Eqs. (25) and (26), and the other governing equations for the source, which are similar to Eqs. (17)–(20), gives expressions for the field variables at all points on the source boundary, which are referred to as the boundary values. The equation for the boundary value $\mathbf{p}^S_{\mathrm{SP}}$, as a function of the excitation $\left(\mathbf{f}_{\mathrm{PH}}^{S}, \mathbf{u}_{\mathrm{SP}}^{S,\mathrm{inc}}, \mathbf{p}_{\mathrm{SP}}^{S,\mathrm{inc}}\right)$ at the source, is

$$\mathbf{p}_{\mathrm{SP}}^{S} = \mathbf{A}^{S}\left(\mathbf{Q}_{1}^{S}\mathbf{H}_{\mathrm{P21}}^{S}\mathbf{f}_{\mathrm{PH}}^{S} + \mathbf{H}_{\mathrm{S22}}^{S}\mathbf{p}_{\mathrm{SP}}^{S,\mathrm{inc}} - \mathbf{u}_{\mathrm{SP}}^{S,\mathrm{inc}}\right) \tag{27}$$

where $\mathbf{A}^{S}$ is similar to $\mathbf{A}$ in Eq. (22). The other boundary values, $\mathbf{u}_{\mathrm{FS}}^{S}$ and $\mathbf{u}_{\mathrm{SP}}^{S}$, can be found by substituting Eq. (27) into Eq. (25) and Eq. (26), respectively.

It is important to note that, for the first iteration, there are no incident fields at the soil-pile interface of the source ($\mathbf{u}_{\mathrm{SP}}^{S,\mathrm{inc}} = \mathbf{p}_{\mathrm{SP}}^{S,\mathrm{inc}} = \mathbf{0}$) because the receiver has not yet been excited. For all subsequent iterations, the expressions for $\mathbf{u}_{\mathrm{SP}}^{S,\mathrm{inc}}$ and $\mathbf{p}_{\mathrm{SP}}^{S,\mathrm{inc}}$ are derived in Eqs. (35) and (36), as detailed below.

Once the boundary values are known for the source excited in isolation, the incident fields that propagate through the soil towards the soil-pile interface of the receiver must be calculated. The modified BEM for internal points is used to calculate these, with the receiver's soil-pile interface regarded as a group of internal points within the domain of the source sub-system. Thus, Eqs. (10) and (11) can be used to calculate the incident displacement $\mathbf{u}_{\mathrm{SP}}^{R,\mathrm{inc}}$ and traction $\mathbf{p}_{\mathrm{SP}}^{R,\mathrm{inc}}$ fields arriving at all $N-1$ piles in the receiver:

$$\mathbf{u}_{\mathrm{SP}}^{R,\mathrm{inc}} = \begin{Bmatrix} \mathbf{u}_{\mathrm{SP}}^{2,\mathrm{inc}} \\ \mathbf{u}_{\mathrm{SP}}^{3,\mathrm{inc}} \\ \vdots \\ \mathbf{u}_{\mathrm{SP}}^{N,\mathrm{inc}} \end{Bmatrix} = \mathbf{G}_{u}^{RS}\begin{Bmatrix} \mathbf{0} \\ \mathbf{p}_{\mathrm{SP}}^{S} \end{Bmatrix} - \mathbf{H}_{u}^{RS}\begin{Bmatrix} \mathbf{u}_{\mathrm{FS}}^{S} \\ \mathbf{u}_{\mathrm{SP}}^{S} \end{Bmatrix} \tag{28}$$

$$\mathbf{p}_{\mathrm{SP}}^{R,\mathrm{inc}} = \begin{Bmatrix} \mathbf{p}_{\mathrm{SP}}^{2,\mathrm{inc}} \\ \mathbf{p}_{\mathrm{SP}}^{3,\mathrm{inc}} \\ \vdots \\ \mathbf{p}_{\mathrm{SP}}^{N,\mathrm{inc}} \end{Bmatrix} = \mathbf{G}_{p}^{RS}\begin{Bmatrix} \mathbf{0} \\ \mathbf{p}_{\mathrm{SP}}^{S} \end{Bmatrix} - \mathbf{H}_{p}^{RS}\begin{Bmatrix} \mathbf{u}_{\mathrm{FS}}^{S} \\ \mathbf{u}_{\mathrm{SP}}^{S} \end{Bmatrix} \tag{29}$$

where the superscript RS denotes that the displacement-state and traction-state matrices containing the transfer functions relating to the propagation of the field variables from the source to the receiver.

3.2.2. The receiver sub-system

This section derives the incident fields that arrive at the soil-pile interface of the source as a result of the scattered field induced at the isolated receiver. The receiver is excited by incident fields that travel from the source, as derived in the previous section. Figure 5 illustrates the BEM meshes used for the receiver sub-system in the same pile-group of two piles, where mesh 3 is used to excite the receiver (pile 2) and mesh 4 is used to find the incident fields at the soil-pile interface of the source (pile 1). The free surface and soil-pile interface of pile 2 is discretised in both meshes, while mesh 4 also defines the soil-pile interface of pile 1 as a group of internal points within the domain of the receiver sub-system.

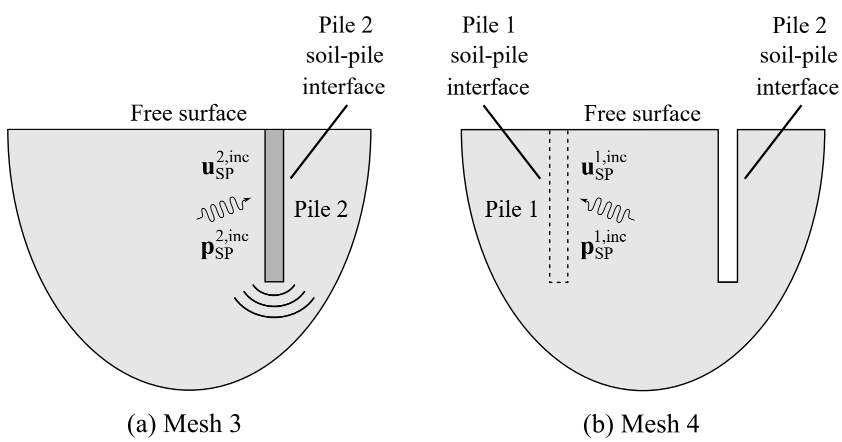

Figure 5: Schematic diagram illustrating the BEM meshes used for the unbounded domain of the isolated receiver sub-system in a pile-group containing two piles. Internal points within the receiver's domain lie along the dashed line in mesh 4. The darker and lighter shaded regions represent material of the pile and soil.

When the BEM is applied using mesh 3, the soil displacement FRF matrix $\mathbf{H}_{\mathrm{S}}^{2}$ around pile 2 can be derived. Similar to Eqs. (23) and (24), the matrix $\mathbf{H}_{\mathrm{S}}^{2}$ can be partitioned into sub-matrices:

$$\left\{\begin{array}{c}\mathbf{u}_{\mathrm{FS}}^{2}\\ \mathbf{u}_{\mathrm{SP}}^{2}-\mathbf{u}_{\mathrm{SP}}^{2,\mathrm{inc}}\end{array}\right\}=\begin{bmatrix}\mathbf{H}_{\mathrm{S11}}^{2} & \mathbf{H}_{\mathrm{S12}}^{2}\\ \mathbf{H}_{\mathrm{S21}}^{2} & \mathbf{H}_{\mathrm{S22}}^{2}\end{bmatrix}\left\{\begin{array}{c}\mathbf{p}_{\mathrm{FS}}^{2}\\ \mathbf{p}_{\mathrm{SP}}^{2}-\mathbf{p}_{\mathrm{SP}}^{2,\mathrm{inc}}\end{array}\right\} \tag{30}$$

where $\mathbf{u}_{\mathrm{FS}}^{2}$ and $\mathbf{p}_{\mathrm{FS}}^{2}=\mathbf{0}$ denote the displacement field and traction-free boundary condition at the free surface of pile 2. As with the source sub-system, there are no incident fields at the free surface. When Eq. (30) is extended to model the BEM mesh of a pile-group containing $N-1$ pile cavities, the resulting soil displacement FRF matrix $\mathbf{H}_{\mathrm{S}}^{R}$ of the receiver can be partitioned into sub-matrices:

$$\begin{Bmatrix} \mathbf{u}_{\mathrm{FS}}^{R} \\ \mathbf{u}_{\mathrm{SP}}^{2} - \mathbf{u}_{\mathrm{SP}}^{2,\mathrm{inc}} \\ \vdots \\ \mathbf{u}_{\mathrm{SP}}^{N} - \mathbf{u}_{\mathrm{SP}}^{N,\mathrm{inc}} \end{Bmatrix} = \begin{bmatrix} \mathbf{H}_{\mathrm{S11}}^{R} & \mathbf{H}_{\mathrm{S12}}^{R} \\ \mathbf{H}_{\mathrm{S21}}^{R} & \mathbf{H}_{\mathrm{S22}}^{R} \end{bmatrix} \begin{Bmatrix} \mathbf{p}_{\mathrm{FS}}^{R} \\ \mathbf{p}_{\mathrm{SP}}^{2} - \mathbf{p}_{\mathrm{SP}}^{2,\mathrm{inc}} \\ \vdots \\ \mathbf{p}_{\mathrm{SP}}^{N} - \mathbf{p}_{\mathrm{SP}}^{N,\mathrm{inc}} \end{Bmatrix}. \tag{31}$$

The rows in Eq. (31) can then be expanded into two governing equations for the soil surrounding the isolated receiver:

$$\mathbf{u}_{\mathrm{FS}}^{R} = \mathbf{H}_{\mathrm{S12}}^{R} \left(\mathbf{p}_{\mathrm{SP}}^{R} - \mathbf{p}_{\mathrm{SP}}^{R,\mathrm{inc}} \right) \tag{32}$$

$$\mathbf{u}_{\mathrm{SP}}^{R} - \mathbf{u}_{\mathrm{SP}}^{R,\mathrm{inc}} = \mathbf{H}_{\mathrm{S22}}^{R} \left(\mathbf{p}_{\mathrm{SP}}^{R} - \mathbf{p}_{\mathrm{SP}}^{R,\mathrm{inc}} \right). \tag{33}$$

Note that the off-diagonal components in the sub-matrix $\mathbf{H}_{\mathrm{S22}}^{R}$ inherently account for the PSPI within the pile-group receiver when the soil is coupled to the piles. This is because all the boundary elements corresponding to the soil cavities of the receiver are used to calculate the transfer functions that fully populate $\mathbf{H}_{\mathrm{S22}}^{R}$.

Similar to Eq. (27), the equation for the boundary value $\mathbf{p}_{\mathrm{SP}}^{R}$, as a function of the excitation $\left(\mathbf{u}_{\mathrm{SP}}^{R,\mathrm{inc}}, \mathbf{p}_{\mathrm{SP}}^{R,\mathrm{inc}} \right)$ at the receiver, is

$$\mathbf{p}_{\mathrm{SP}}^{R} = \mathbf{A}^{R} \left(\mathbf{H}_{\mathrm{S22}}^{R} \mathbf{p}_{\mathrm{SP}}^{R,\mathrm{inc}} - \mathbf{u}_{\mathrm{SP}}^{R,\mathrm{inc}} \right). \tag{34}$$

The other boundary values, $\mathbf{u}_{\mathrm{FS}}^{R}$ and $\mathbf{u}_{\mathrm{SP}}^{R}$, are found by substituting Eq. (34) into Eq. (32) and Eq. (33), respectively.

Once the boundary values at the receiver are known, Eqs. (10) and (11) are used to calculate the incident displacement $\mathbf{u}_{\mathrm{SP}}^{S,\mathrm{inc}}$ and traction $\mathbf{p}_{\mathrm{SP}}^{S,\mathrm{inc}}$ fields at the soil-pile interface of the source pile, which are defined by the internal points within the domain of the receiver:

$$\mathbf{u}_{\mathrm{SP}}^{S,\mathrm{inc}} = \mathbf{u}_{\mathrm{SP}}^{1,\mathrm{inc}} = \mathbf{G}_{u}^{SR} \begin{Bmatrix} \mathbf{0} \\ \mathbf{p}_{\mathrm{SP}}^{R} \end{Bmatrix} - \mathbf{H}_{u}^{SR} \begin{Bmatrix} \mathbf{u}_{\mathrm{FS}}^{R} \\ \mathbf{u}_{\mathrm{SP}}^{R} \end{Bmatrix} \tag{35}$$

$$\mathbf{p}_{\mathrm{SP}}^{S,\mathrm{inc}} = \mathbf{p}_{\mathrm{SP}}^{1,\mathrm{inc}} = \mathbf{G}_p^{SR} \begin{Bmatrix} \mathbf{0} \\ \mathbf{p}_{\mathrm{SP}}^{R} \end{Bmatrix} - \mathbf{H}_p^{SR} \begin{Bmatrix} \mathbf{u}_{\mathrm{FS}}^{R} \\ \mathbf{u}_{\mathrm{SP}}^{R} \end{Bmatrix} \tag{36}$$

where the superscript SR denotes the displacement-state and traction-state matrices containing the transfer functions relating to the propagation of the field variables from the receiver to the source.

4. Validation

In this section, results predicted using the direct and indirect methods are compared against published results for the dynamic interaction factors for two neighbouring piles. Both piles have the same material properties and dimensions, with pile diameter d and centre-to-centre pile separation s, as shown in Fig. 6. All results are computed by implementing the equations of Section 3 using the technical computing software, MATLAB [22].

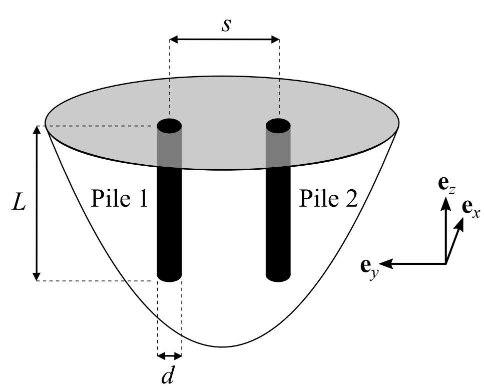

Figure 6: Schematic diagram of two neighbouring piles, with equal length L and diameter d, and centre-to-centre separation s.

The dynamic interaction factors α_{ij} between two piles in isolation are defined as

$$\alpha_{ij} = \frac{\text{Dynamic motion } i \text{ at pile-head 2 due to load } j \text{ at pile-head 1}}{\text{Static motion } i \text{ at pile-head 1 due to load } j \text{ at pile-head 1}} \,. \tag{37}$$

These can also be expressed as functions of the following non-dimensional groups:

$$\alpha_{ij} = g_{ij}\left(a_0, \frac{L}{d}, \frac{s}{d}, \frac{E_s}{E_p}, \frac{\rho_s}{\rho_p}, \nu_p, \nu_s, \eta_s\right) \tag{38}$$

where $a_0 = \omega d/c_S$ is the non-dimensional frequency, $c_S = \sqrt{G_s/\rho_s}$ is the shear wave speed in the soil and $E_s = 2G_s(1+\nu_s)$. For typical London Clay, $G_s = 96$ MPa and $\rho_s = 1980\ \mathrm{kg/m^3}$, giving $c_S = 220$ m/s [23].

Figure 7 plots the real and imaginary parts of six dynamic interaction factors against a_0, using Kaynia's model [7] and both the direct and indirect methods, for different pile separation ratios ($s/d = 2, 5, 10$). The non-dimensional soil and pile parameters are: $L/d = 15$, $E_s/E_p = 10^{-3}$, $\rho_s/\rho_p = 0.7$, $\nu_p = 0.25$, $\nu_s = 0.4$ and $\eta_s = 0.05$. Note that Kaynia's results are only plotted for frequencies up to $a_0 = 1.0$ ($\approx$ 50 Hz for London Clay). The results from the direct and indirect methods are plotted up to $a_0 = 3.2$ ($\approx$ 160 Hz), to include the frequency range of interest for ground-borne vibration. The complex nature of the interaction factors accounts for the phase difference between the applied force and the resulting displacements. Hence, under static loading, there is no phase difference and the interaction factors are purely real.

There is very good agreement between the results from all three methods. The reciprocity relationships for $\alpha_{\phi_x f_y} = \alpha_{u_y q_x}$ and $\alpha_{\phi_y f_x} = \alpha_{u_x q_y}$ (omitted in Fig. 7 for conciseness) are also satisfied. For piles in close proximity to each other ($s/d = 2$), and when $a_0 > 1.2$, two iterations are required for the indirect method to converge with the direct method when the excitation is either the force f_y or moment q_x. These both result in pile deflections in the direction of the propagating waves between the piles, which means that the incident fields are more likely to be influenced by the presence of the receiver. For all other interaction factors, just one iteration is sufficient for convergence. Indeed, one iteration, which is equivalent to the uncoupled source-receiver model, may be regarded as providing a good approximation for all interactions factors over the frequency range of interest.

As expected, the influence of the receiver on the pile-group response decreases with increasing pile separation: when $s/d \geq 5$, one iteration is sufficient for convergence across the frequency range. Note that, in general, as the pile separation is increased, the magnitude of the interaction factors decreases due to increased attenuation in the soil. Furthermore, the number of peaks and troughs in the factors increases as the number of half-wavelengths in the soil between the piles

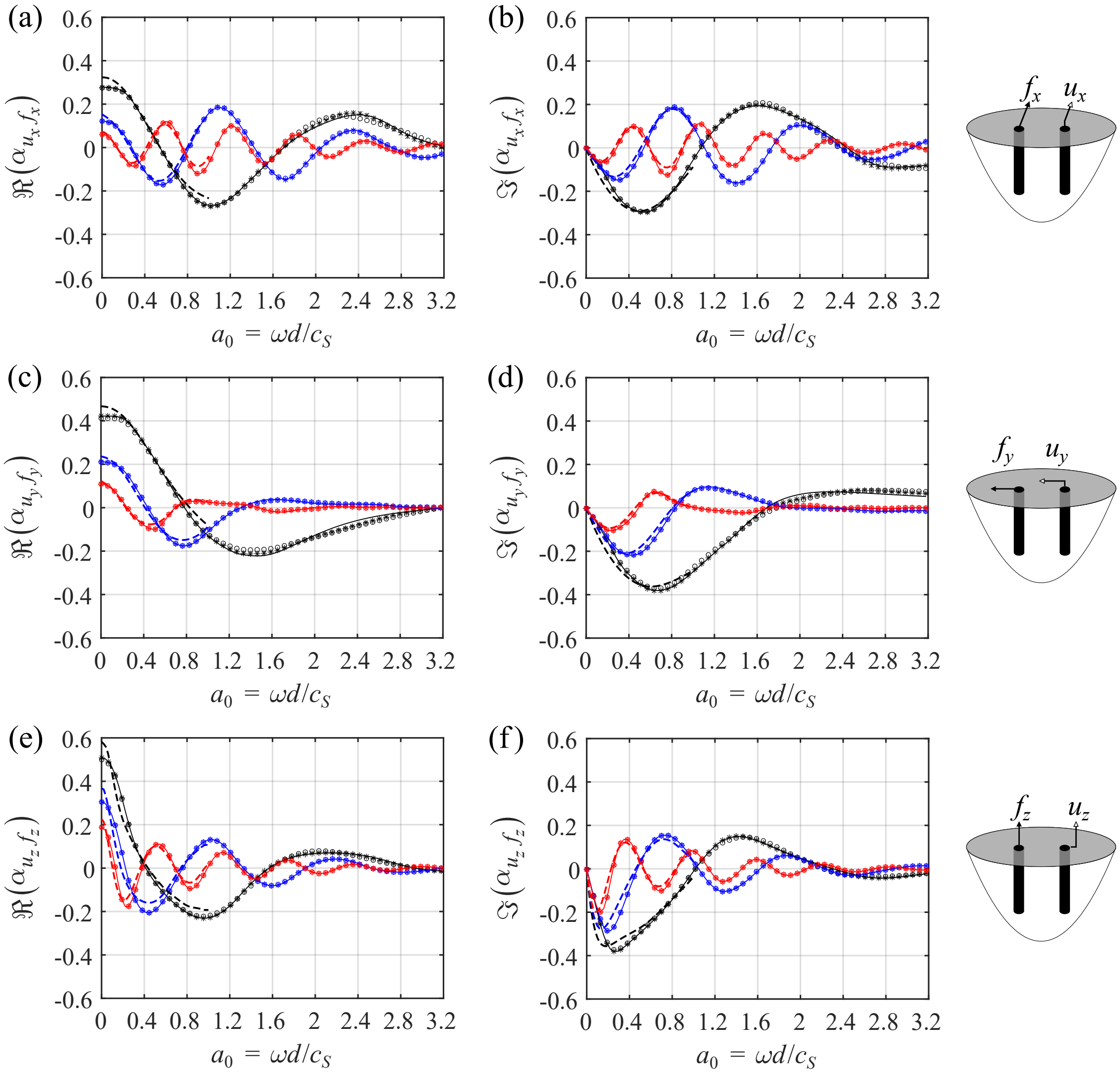

Figure 7: Continues over page.

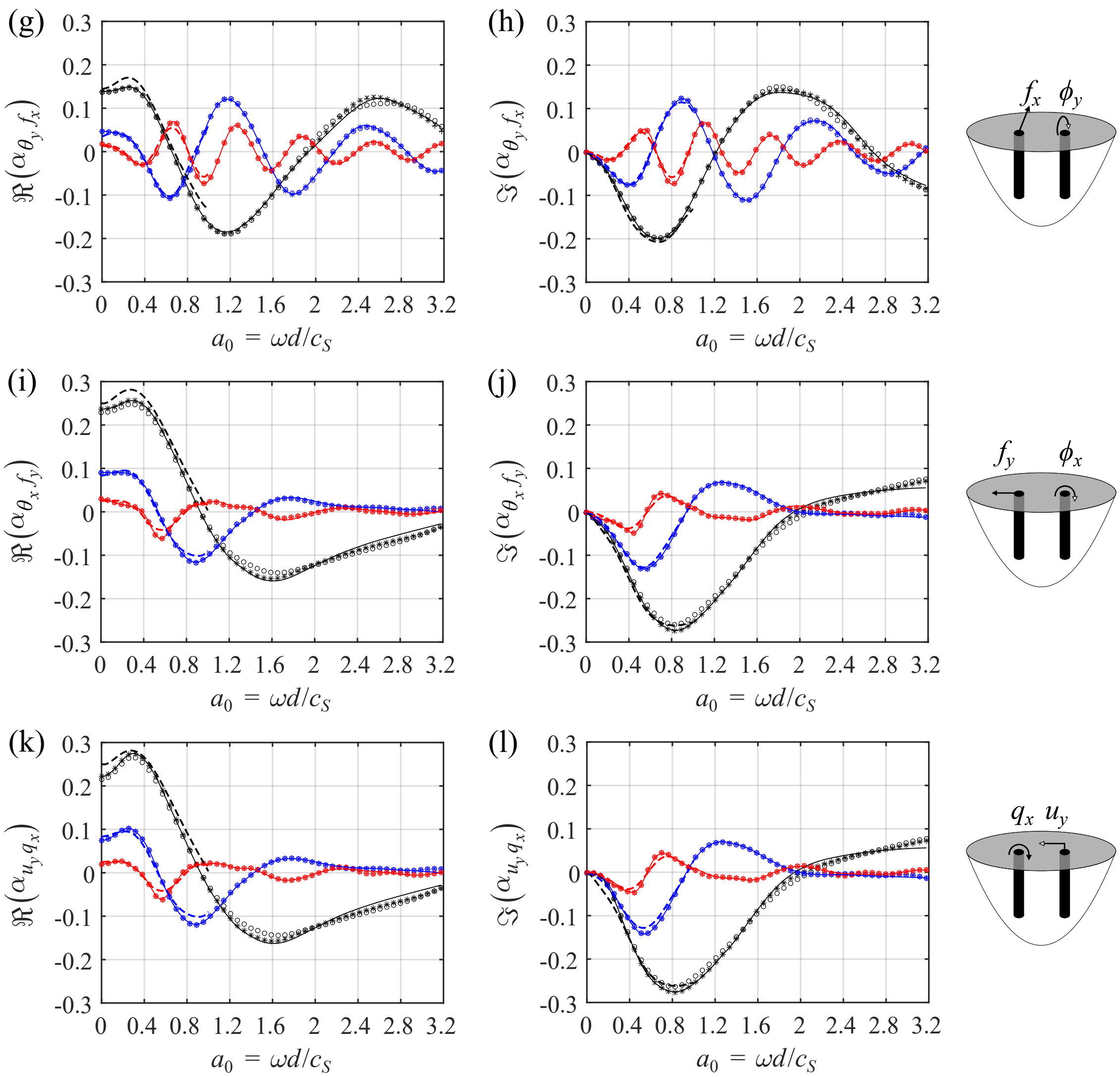

s/d	Kaynia	DM	IM (iterations) 1	2	3
2	black dashed line	black solid line	○	+	×
5	blue dashed line	blue solid line	○	+	×
10	red dashed line	red solid line	○	+	×

Figure 7: The real and imaginary parts of six dynamic interaction factors plotted against non-dimensional frequency a_0 for two neighbouring piles with different pile separation ratios $(s/d = 2, 5, 10)$. The responses are predicted using Kaynia's model, the direct method (DM) and the indirect method (IM), for non-dimensional soil and pile parameters $L/d = 15$, $E_s/E_p = 10^{-3}$, $\rho_s/\rho_p = 0.7$, $\nu_p = 0.25$, $\nu_s = 0.4$ and $\eta_s = 0.05$.

increases, leading to more incidences of constructive and destructive interference.

5. Parametric Study

This section investigates the influence of different material parameters, and of neighbouring and intermediate piles, by focusing on the lateral ($\alpha_{u_x f_x}, \alpha_{u_y f_y}$) and vertical ($\alpha_{u_z f_z}$) interaction factors. All piles in the pile-group are separated by $s/d = 2$, and the results are predicted using both the direct and indirect methods. Typical non-dimensional parameters for concrete piles embedded in London Clay are specified: $E_s/E_p = 1.4 \times 10^{-2}$, $\rho_s/\rho_p = 0.8$, $\nu_s = 0.49$, $\nu_p = 0.15$ and $\eta_s = 0.08$.

5.1. Influence of the soil-to-pile stiffness ratio E_s/E_p

Figure 8 plots the interaction factors predicted for two neighbouring piles for a range of soil-to-pile stiffness ratios, from flexible ($E_s/E_p = 10^{-2}$, 10^{-3}) to effectively rigid ($E_s/E_p = 10^{-4}$, 10^{-5}) piles. In all cases, the first iteration of the indirect method provides a good approximation to the direct method, even at high frequencies. This implies that varying the stiffness ratio does not have a significant influence on the wave-scattering effect.

The effect of the stiffness ratio on the lateral factors, $\alpha_{u_x f_x}$ and $\alpha_{u_y f_y}$, is to reduce the static and low-frequency ($a_0 < 0.8$) amplitudes as the piles become more flexible (i.e. E_s/E_p increases). For $a_0 > 0.8$, the effect becomes less significant. In contrast, there is almost no change in $\alpha_{u_z f_z}$ over the frequency range of interest, except with very flexible piles ($E_s/E_p = 10^{-2}$). In this case, the increased flexibility reduces the amplitude across the frequency range, although the frequencies at which the peaks and troughs occur do not shift when $a_0 < 2.0$.

5.2. Influence of the soil-to-pile density ratio ρ_s/ρ_p

The interaction factors predicted for two neighbouring piles with different soil-to-pile density ratios, corresponding to light ($\rho_s/\rho_p = 1.0$) and dense ($\rho_s/\rho_p = 0.7, 0.4$) piles, are plotted in Fig. 9. As expected, the static and low-frequency ($a_0 < 0.8$) amplitudes of all interaction factors are independent of ρ_s/ρ_p because inertial effects are insignificant at these frequencies. For ρ_s/ρ_p between 1.0 and 0.7, there is also no discernible effect at higher frequencies, which agrees with results published by Gazetas et al. [18] using Kaynia's model [7]. Reducing the density ratio further, to $\rho_s/\rho_p = 0.4$, causes two effects at higher frequencies: (1) an increase in the interaction factor amplitudes; and (2) a decrease in the frequencies at which the peaks and troughs in the factors occur. In physical terms, lighter soils offer less resistance to the piles, leading to higher amplitude waves in the soil. For the densest piles ($\rho_s/\rho_p = 0.4$), at high frequencies ($a_0 > 1.2$), two iterations of the indirect method are required for convergence, which is consistent with the wave-scattering effect being most significant when there is a large difference in mechanical impedance between the soil and piles.

5.3. Influence of neighbouring and intermediate piles

In order to identify if neighbouring and intermediate piles can influence the wave-scattering effect, the definition of the dynamic interaction factors for two isolated piles, given in Eq. (37), needs to be extended to a generic pile-group. The corresponding factors α_{ij}^{ab} between any two piles a and b in a generic pile-group are therefore defined as

$$\alpha_{ij}^{ab} = \frac{\text{Dynamic motion } i \text{ at pile-head } a \text{ due to load } j \text{ at pile-head } b}{\text{Static motion } i \text{ at pile-head } b \text{ due to load } j \text{ at pile-head } b}\,. \tag{39}$$

It is expected that the wave-scattering effect will have a greater influence on the PSPI between any two piles when the number of neighbouring piles increases. This is due to an increase in the distribution of waves propagating back-and-forth between piles within the group and a greater propensity for wave interference than is present with only two isolated piles.

Figure 10 plots the interaction factors for two adjacent piles (piles 1 and 2) when the number of neighbouring piles is increased from a 1×2 pile-group to a 3×3 pile-group. Slight changes are observed, especially at high frequencies ($\alpha_0 > 1.6$), and these coincide with an increase in the number of iterations required for the indirect method to converge, which is consistent with the expected increase in wave scattering. For example, when $a_0 > 1.4$, the vertical interaction factor $\alpha_{u_z f_z}^{21}$ requires two iterations for convergence when the number of piles is increased from a 1×2 to a 2×2 pile-group. Nevertheless, these changes are not significant, and it is clear that an isolated

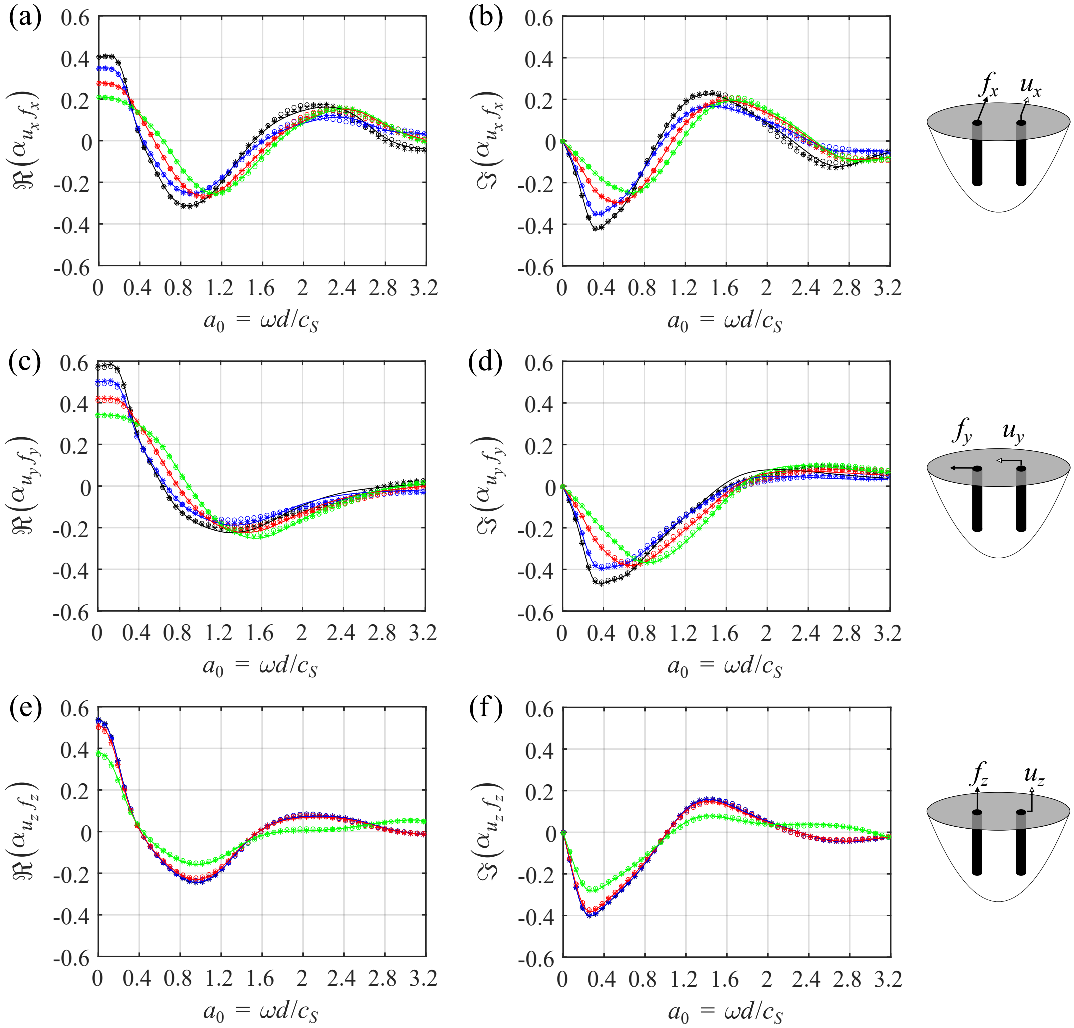

E_s/E_p	DM	IM (iterations) 1	2	3
10^{-5}	—— (black)	○	+	×
10^{-4}	—— (blue)	○	+	×
10^{-3}	—— (red)	○	+	×
10^{-2}	—— (green)	○	+	×

Figure 8: The real and imaginary parts of the (a)–(d) lateral and (e)–(f) vertical dynamic interaction factors plotted against non-dimensional frequency a_0 for two neighbouring piles with different soil-to-pile stiffness ratios ($E_s/E_p =$ 10^{-5}, 10^{-4}, 10^{-3}, 10^{-2}). The responses are predicted using the direct method (DM) and the indirect method (IM), for non-dimensional soil and pile parameters $L/d = 15$, $s/d = 2$, $\rho_s/\rho_p = 0.7$, $\nu_p = 0.25$, $\nu_s = 0.4$ and $\eta_s = 0.05$.

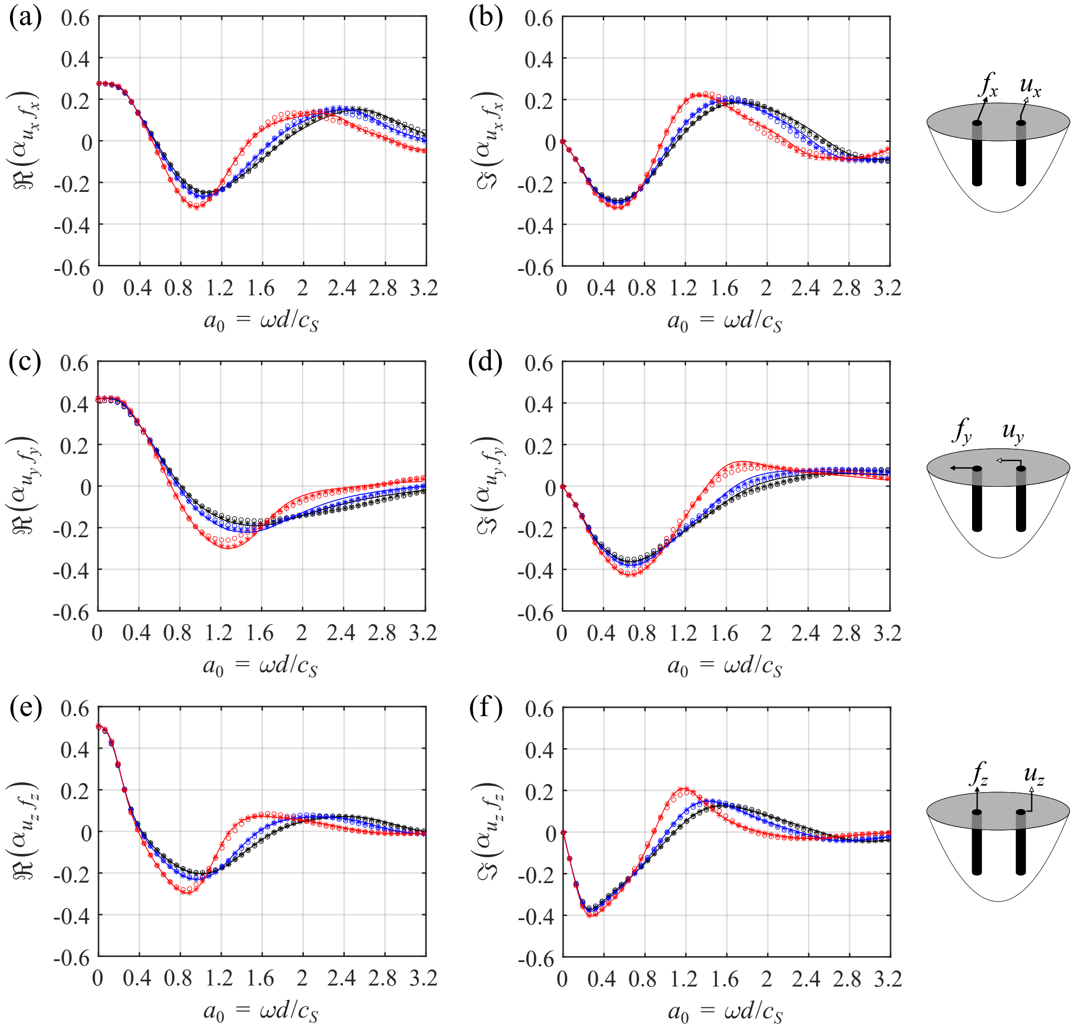

ρ_s/ρ_p	DM	IM (iterations) 1	2	3
1.0	—— (black)	○	+	×
0.7	—— (blue)	○	+	×
0.4	—— (red)	○	+	×

Figure 9: The real and imaginary parts of the (a)–(d) lateral and (e)–(f) vertical dynamic interaction factors plotted against non-dimensional frequency a_0 for two neighbouring piles with different soil-to-pile density ratios ($\rho_s/\rho_p = 1.0,\ 0.7,\ 0.4$). The responses are predicted using the direct method (DM) and the indirect method (IM), for non-dimensional soil and pile parameters $L/d = 15$, $s/d = 2$, $E_s/E_p = 10^{-3}$, $\nu_p = 0.25$, $\nu_s = 0.4$ and $\eta_s = 0.05$.

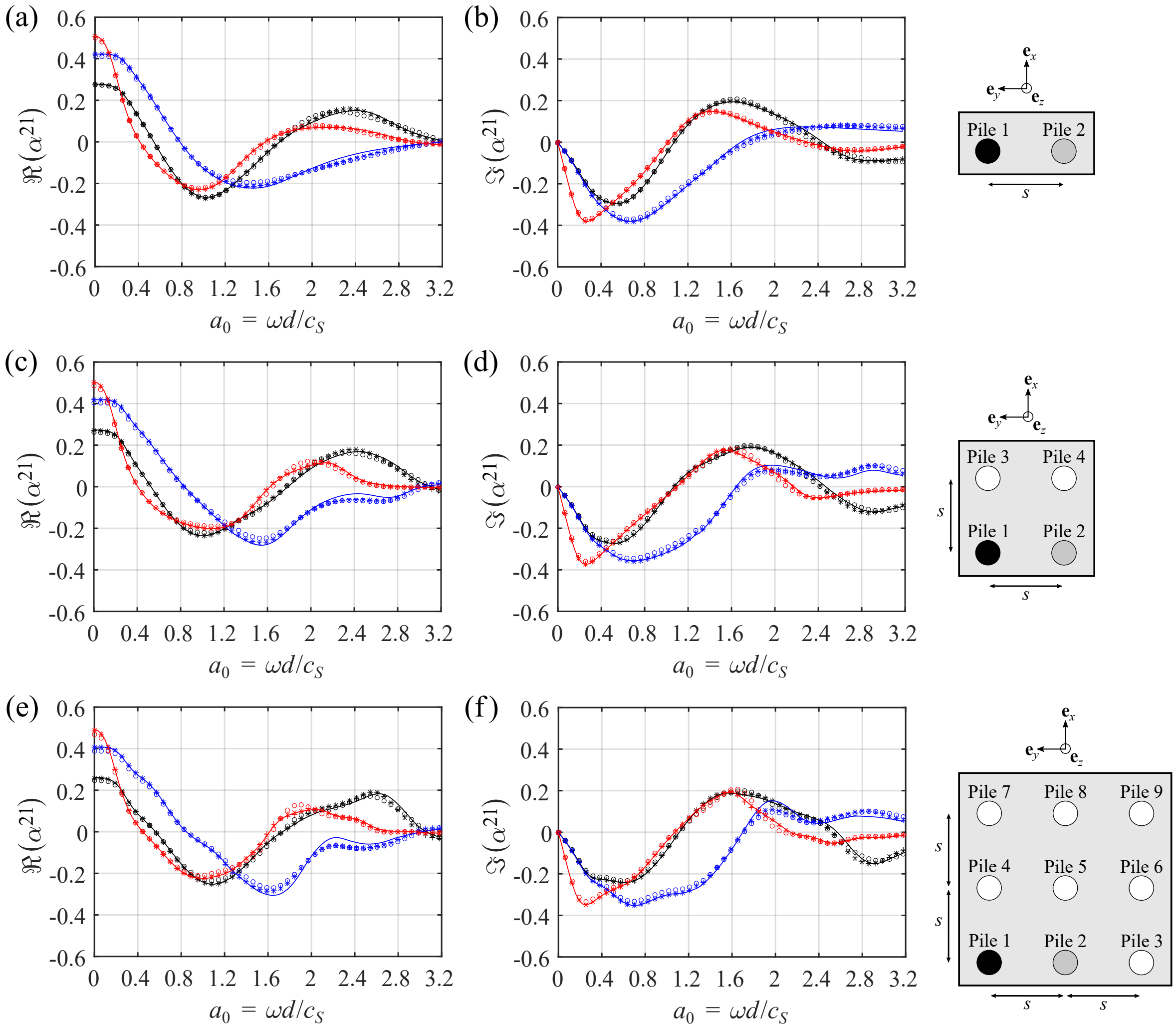

α^{21}	DM	IM (iterations) 1	2	3
$u_x f_x$	——	○	+	×
$u_y f_y$	——	○	+	×
$u_z f_z$	——	○	+	×

Figure 10: The real and imaginary parts of the lateral and vertical dynamic interaction factors plotted against non-dimensional frequency a_0 for two adjacent piles in a (a)–(b) 1×2, (c)–(d) 2×2 and (e)–(f) 3×3 pile-group. In each pile-group, pile 1 (shaded black) is excited and the displacement calculated at pile 2 (shaded grey) to give α^{21}, using the direct method (DM) and the indirect method (IM), for non-dimensional soil and pile parameters $L/d = 15$, $s/d = 2$, $E_s/E_p = 10^{-3}$, $\rho_s/\rho_p = 0.4$, $\nu_p = 0.25$, $\nu_s = 0.4$ and $\eta_s = 0.05$.

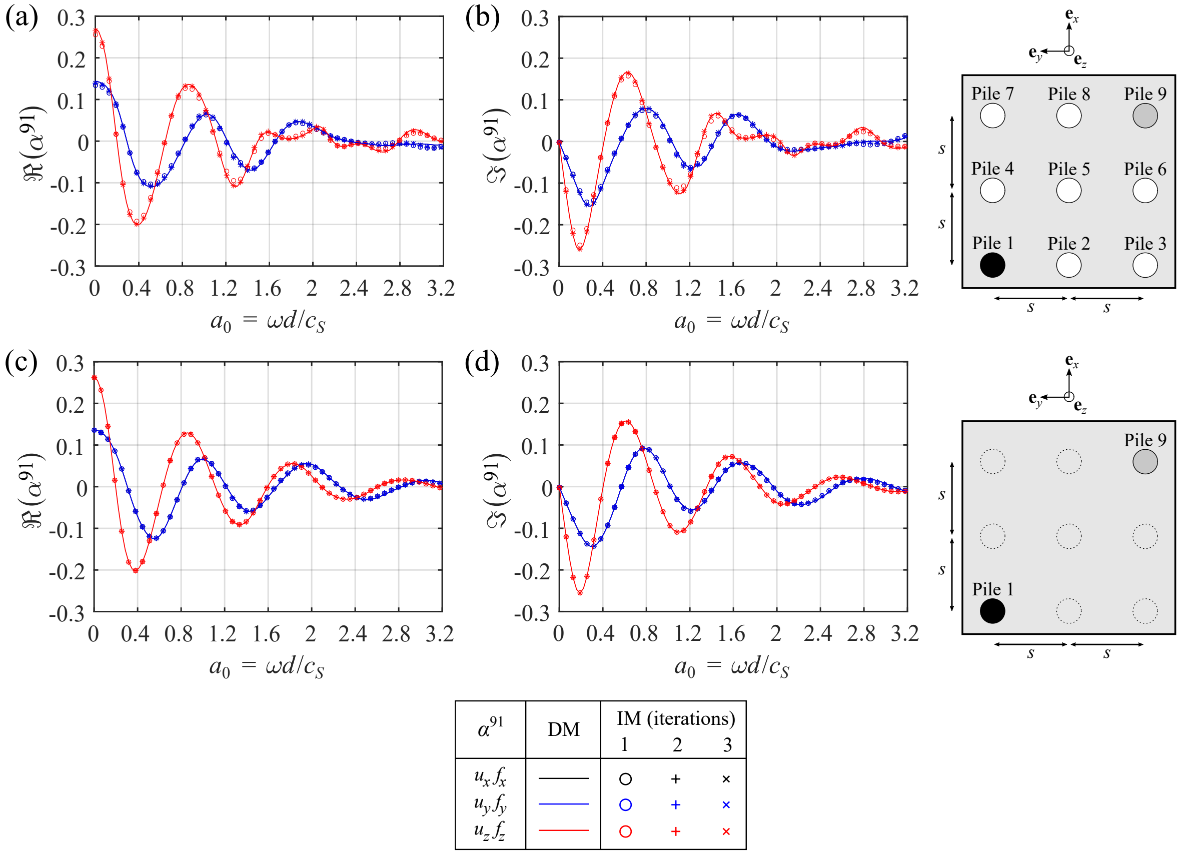

Figure 11: The real and imaginary parts of the lateral and vertical dynamic interaction factors plotted against non-dimensional frequency a_0 for two diagonally opposite piles in a 3×3 pile-group, when the presence of intermediate piles is (a)–(b) included and (c)–(d) omitted. In each case, pile 1 (shaded black) is excited and the displacement is calculated at pile 9 (shaded grey) to give α^{91}, using the direct method (DM) and the indirect method (IM), for non-dimensional soil and pile parameters $L/d = 15$, $s/d = 2$, $E_s/E_p = 10^{-3}$, $\rho_s/\rho_p = 0.4$, $\nu_p = 0.25$, $\nu_s = 0.4$ and $\eta_s = 0.05$.

two-pile model provides a good approximation, across the frequency range, for the interaction factors of larger pile-groups.

In contrast, the influence of intermediate piles is more significant. Figure 11 plots the corresponding results for two diagonally opposite piles (piles 1 and 9) in a 3×3 pile-group when the intermediate piles are either included or omitted. Note that the lateral interaction factors $\alpha^{91}_{u_x f_x}$ and $\alpha^{91}_{u_y f_y}$ are equivalent in Fig. 11 because piles 1 and 9 are positioned at $45°$ to the x and y axes. There is no discernible difference between the two sets of results at low and intermediate frequencies ($a_0 < 1.2$). At higher frequencies, when the intermediate piles are included, the peaks and troughs in the interaction factors shift to lower frequencies and increase in number. In physical terms, when pile 1 is excited, the wave-fields that arrive at pile 9 are scattered by the intermediate piles with a different phase. Note that, in this case, the wave-scattering effect is captured well with just one iteration because the intermediate piles and pile 9 are together regarded as the receiver sub-system (i.e. all the piles in the receiver are coupled together).

Based on these observations, it is clear that the PSPI between two piles in a large pile-group can indeed be approximated by ignoring neighbouring piles, even at the higher frequencies associated with ground-borne vibration (1–160 Hz), provided the two piles are adjacent to each other. This approximation is also valid when intermediate piles are present but only up to moderate frequencies (≈ 60 Hz). At higher frequencies, when the soil wavelengths approach the length scale of the pile diameter, the scattered fields generated at the intermediate piles are more significant and influence the PSPI to a greater extent.

6. Conclusions

This paper has considered the dynamic behaviour of pile-groups under inertial loading, when excited by loads applied at a single pile-head. Results are presented over a range of non-dimensional frequencies a_0, which correspond to ground-borne vibration in London Clay in the range $1 - 160$ Hz. An indirect method has been developed, based on an iterative wave-scattering approach, to couple the piles in a source-receiver BEM model. This has been shown to offer an effective alternative to a direct method based on a standard BEM model of a complete pile-group. By comparing dynamic interaction factors, the two methods have been shown to agree very well, and the indirect method has provided useful insights into the significance of wave scattering between piles.

In general, the first iteration of the indirect method provides a good approximation for the coupled response as the pile separation ratio s/d, soil-to-pile stiffness ratio E_s/E_p and soil-to-pile density ratio ρ_s/ρ_p are all varied; even at frequencies well above those of previously published results. These results show that dynamic interaction factors, calculated using uncoupled source-receiver models, can account effectively for the pile-soil-pile interaction (PSPI) between piles without resorting to fully coupled models. An isolated two-pile model provides a good approximation, across the frequency range, for the interaction factors between adjacent piles in larger pile-groups, although the presence of intermediate piles may need to be considered at high frequencies because of the increased influence of wave scattering that these introduce.

A fundamental assumption in this study is that the ground may be represented as a homogeneous half-space, but this is often not the case due to soil layering. Layering introduces additional wave reflections and mode conversions, and this is likely to affect the PSPI at the high frequencies associated with ground-borne vibration. The extent to which this is the case remains the subject of future research.

References

[1] J. P. Talbot. “Base-isolated buildings: towards performance-based design”. In: *Proceedings of the Institution of Civil Engineers - Structures and Buildings* 169.8 (2016), pp. 574–582. DOI: 10.1680/jstbu.15.00057.

[2] K. A. Kuo and H. E. M. Hunt. “Dynamic models of piled foundations”. In: *Applied Mechanics Reviews* 65.3 (2013), pp. 031003 1–9. DOI: 10.1115/1.4024675.

[3] G. Gazetas and R. Dobry. “Horizontal response of piles in layered soils”. In: *Journal of Geotechnical Engineering* 110.1 (1984), pp. 20–40. DOI: 10.1061/(ASCE)0733-9410(1984)110:1(20).

[4] R. Dobry and G. Gazetas. “Simple method for dynamic stiffness and damping of floating pile groups”. In: *Géotechnique* 38.4 (1988), pp. 557–574. DOI: 10.1680/geot.1988.38.4.557.

[5] G. Gazetas and N. Makris. “Dynamic pile-soil-pile interaction. Part I: Analysis of axial vibration”. In: *Earthquake Engineering & Structural Dynamics* 20.2 (1991), pp. 115–132. DOI: 10.1002/eqe.4290200203.

[6] N. Makris and G. Gazetas. “Dynamic pile-soil-pile interaction. Part II: Lateral and seismic response”. In: *Earthquake Engineering & Structural Dynamics* 21.2 (1992), pp. 145–162. DOI: 10.1002/eqe.4290210204.

[7] A. M. Kaynia. “Dynamic Stiffness and Seismic Response of Pile Groups”. PhD thesis. Massachusetts Institute of Technology, U.S.A., 1982.

[8] A. M. Kaynia and E. Kausel. “Dynamic behaviour of pile groups”. In: *Proceedings of the 2nd International Conference on Numerical Methods in Offshore Piling*. Austin, Texas, USA, 1982, pp. 509–532.

[9] S. M. Mamoon, A. M. Kaynia, and P. K. Banerjee. “Frequency Domain Dynamic Analysis of Piles and Pile Groups”. In: *Journal of Engineering Mechanics* 116.10 (1990), pp. 2237–2257. DOI: 10.1061/(ASCE)0733-9399(1990)116:10(2237).

[10] P. A. Martin. *Multiple Scattering: Interaction of Time-Harmonic Waves with N Obstacles*. Encyclopedia of Mathematics and its Applications. Cambridge, U.K.: Cambridge University Press, 2006. DOI: 10.1017/CBO9780511735110.

[11] J. G. Fikioris and P. C. Waterman. “Multiple scattering of waves. Part III: The electromagnetic case”. In: *Journal of Quantitative Spectroscopy and Radiative Transfer* 123 (2013), pp. 8–16. DOI: 10.1016/J.JQSRT.2012.09.007.

[12] A. K. Hamid and M. I. Hussein. “Iterative solution to the electromagnetic plane wave scattering by two parallel conducting elliptic cylinders”. In: *Journal of Electromagnetic Waves and Applications* 17.6 (2003), pp. 813–828. DOI: 10.1163/156939303322503376.

[13] J. G. Fikioris and P. C. Waterman. “Multiple scattering of waves. Part II: ’Hole corrections’ in the scalar case”. In: *Journal of Mathematical Physics* 5 (1964), p. 1413. DOI: 10.1063/1.1704077.

[14] X. Li and J. A. Hudson. “Multiple scattering of elastic waves from a continuous and heterogeneous region”. In: *Geophysical Journal International* 126 (1996), pp. 845–862. DOI: 10.1111/j.1365-246X.1996.tb04707.x.

[15] T. E. Doyle. “Iterative simulation of elastic wave scattering in arbitrary dispersions of spherical particles”. In: *The Journal of the Acoustical Society of America* 119 (2006), pp. 2599–2610. DOI: 10.1121/1.2184989.

[16] T. L. Edirisinghe, J. P. Talbot, and M. F. M. Hussein. “Accounting for the influence of the free surface on the vibration response of underground railway tunnels: a new iterative method”. In: *Proceedings of the 29th International Conference on Noise and Vibration Engineering and USD*. Leuven, Belgium, 2020.

[17] G. Gazetas. “Soil Dynamics: An Overview”. In: *Dynamic Behaviour of Foundations and Buried Structures: Vol. 3*. Ed. by P K Banerjee and R Butterfield. Elsevier Applied Science, 1987. Chap. 1.

[18] G. Gazetas, K. Fan, A. M. Kaynia, et al. “Dynamic interaction factors for floating pile groups”. In: *Journal of Geotechnical Engineering* 117.10 (1991), pp. 1531–1548. DOI: 10.1061/(ASCE)0733-9410(1991)117:10(1531).

[19] J. P. Talbot and H. E. M. Hunt. “A computationally efficient piled-foundation model for studying the effects of ground-borne vibration on buildings”. In: *Proceedings of the Institution of Mechanical Engineers, Part C: Journal of Mechanical Engineering Science* 217.9 (2003), pp. 975–989. DOI: 10.1243/095440603322407227.

[20] P. Coulier, G. Degrande, K. A. Kuo, et al. “A comparison of two models for the vibration response of piled foundations to inertial and underground-railway-induced loadings”.

In: *Proceedings of the 17th International Congress on Sound and Vibration*. Vol. 2. Cairo, Egypt: International Institute of Acoustics and Vibration, 2010, pp. 1512–1519.

[21] J. Domínguez. *Boundary Elements in Dynamics*. Southampton & Essex, U.K.: Computational Mechanics Publications & Elsevier Applied Science, 1993.

[22] MathWorks Ltd. MATLAB, Version 9.7, R2019b, Cambridge, U.K., 2019.

[23] D. W. Hight, F. McMillan, J. J. M. Powell, et al. "Some characteristics of London clay". In: *Characterisation & Engineering Properties of Natural Soils*. Ed. by T S Tan, K K Phoon, David W Hight, et al. Vol. 2. Tokyo, Japan: Balkema, 2003, pp. 851–907.

[24] J. J. Rego Silva, H. Power, and L. C. Wrobel. "A boundary element method for 3D time-harmonic elastodynamics - Numerical aspects". In: *Boundary Elements XV Vol 2 Stress Analysis*. WIT Press, 1993, pp. 423–439.

Appendix A. The boundary-element method (BEM) for internal points

Consider a homogeneous, isotropic, three-dimensional domain Ω with surface Γ. When an internal point $\mathbf{y} \in \Omega$ lies on the surface Γ_y of sub-domain Ω_y, where $\Omega_y \subset \Omega$, as shown in Fig. A.1, the integral equation that represents the displacement-state at $\mathbf{y}$ is derived by Domínguez [21]:

$$u_l\left(\mathbf{y}\right) + \int_\Gamma p^*_{lk}\left(\mathbf{y},\mathbf{x}\right) u_k\left(\mathbf{x}\right) d\Gamma = \int_\Gamma u^*_{lk}\left(\mathbf{y},\mathbf{x}\right) p_k\left(\mathbf{x}\right) d\Gamma \tag{A.1}$$

where u^*_{lk} and p^*_{lk} are second-order tensors, or matrices, that represent the fundamental solutions of the displacement-state between the integration point vector $\mathbf{y}$ in the domain and the collocation point vector $\mathbf{x}$ at the domain surface.

The closed-form expressions for u^*_{lk} and p^*_{lk} [21] are:

$$u^*_{lk} = \frac{1}{4\pi\rho c_S^2}, \left(\psi\delta_{lk} - \chi r_{,l} r_{,k}\right) \tag{A.2}$$

$$p^*_{lk} = \frac{1}{4\pi}\left[A\left(\frac{\partial r}{\partial n}\delta_{lk} + n_l r_{,k}\right) + B r_{,l} r_{,k}\frac{\partial r}{\partial n} + C r_{,l} n_k\right] \tag{A.3}$$

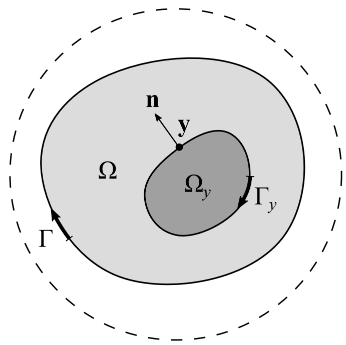

Figure A.1: The domain Ω (lighter shaded region) with boundary surface Γ is defined within an infinite domain, represented by the dashed line. The internal point $\mathbf{y} \in \Omega$, with normal unit-vector $\mathbf{n}$, lies on the surface Γ_y separating the sub-domain Ω_y (darker shaded region) from Ω.

where ρ is the mass density, $r = |\mathbf{y} - \mathbf{x}|$ is the distance between the integration and collocation points, δ_{lk} is the Kronecker delta, and n_l is the unit normal vector in the direction $\mathbf{e}_l$. Equations (A.2) and (A.3) are expressed in terms of the following variables:

$$\psi = \frac{e^{-k_S r}}{r}\left(1 + \frac{1}{k_S r} + \frac{1}{{k_S}^2 r^2}\right) - \frac{e^{-k_P r}}{r}\frac{{c_S}^2}{{c_P}^2}\left(1 + \frac{1}{k_P r} + \frac{1}{{k_P}^2 r^2}\right) \tag{A.4}$$

$$\chi = \frac{e^{-k_S r}}{r}\left(1 + \frac{3}{k_S r} + \frac{3}{{k_S}^2 r^2}\right) - \frac{e^{-k_P r}}{r}\frac{{c_S}^2}{{c_P}^2}\left(1 + \frac{3}{k_P r} + \frac{3}{{k_P}^2 r^2}\right) \tag{A.5}$$

$$A = \frac{d\psi}{dr} - \frac{\chi}{r} \tag{A.6}$$

$$B = 4\frac{\chi}{r} - 2\frac{d\chi}{dr} \tag{A.7}$$

$$C = \frac{\lambda}{\mu}\left(\frac{d\psi}{dr} - \frac{d\chi}{dr} - 2\frac{\chi}{r}\right) - 2\frac{\chi}{r} \tag{A.8}$$

with wavenumbers

$$k_{P,S} = \frac{i\omega}{c_{P,S}} \tag{A.9}$$

and phase speeds

$$c_P = \sqrt{\frac{\lambda + 2\mu}{\rho}} \tag{A.10}$$

$$c_S = \sqrt{\frac{\mu}{\rho}} \tag{A.11}$$

where λ and μ are the elastic Lamé constants, and the subscripts P and S denote variables associated with the pressure and shear waves, respectively.

By numerically computing the integrals in Eq. (A.1) using standard Gauss-Legendre quadrature, and assuming the field variables are uniform at the collocation points, the displacement $u_l(\mathbf{y}_i)$ at multiple M internal points can be rewritten as

$$\begin{aligned} u_l\left(\mathbf{y}_i\right) + \sum_{j=1}^{N} \left(\int_{\Gamma_j} p_{lk}^{*}\left(\mathbf{y}_i, \mathbf{x}_j\right) d\Gamma_j \right) u_k\left(\mathbf{x}_j\right) = \\ \sum_{j=1}^{N} \left(\int_{\Gamma_j} u_{lk}^{*}\left(\mathbf{y}_i, \mathbf{x}_j\right) d\Gamma_j \right) p_k\left(\mathbf{x}_j\right) \quad \text{for } i = 1, 2, \ldots, M \end{aligned} \tag{A.12}$$

when there are N nodes at the domain surface. It is worth noting that the integral formulation used in the standard BEM requires numerical schemes to avoid the weak and strong singularities in u_{lk}^{*} and p_{lk}^{*}, respectively, when $\mathbf{y}_i = \mathbf{x}_j$. These singularities are not present when finding the response at internal points because the integration and collocation points never coincide with each other.

The generalised Hooke's Law for an isotropic continuum and Cauchy's formula are applied to Eq. (A.12) to get an integral equation for the traction $p_l(\mathbf{y}_i)$ [24] at M internal nodes:

$$\begin{aligned} p_l\left(\mathbf{y}_i\right) + \sum_{j=1}^{N} \left(\int_{\Gamma_j} p_{lmk}^{*}\left(\mathbf{y}_i, \mathbf{x}_j\right) n_m\left(\mathbf{y}_i\right) d\Gamma_j \right) u_k\left(\mathbf{x}_j\right) = \\ \sum_{j=1}^{N} \left(\int_{\Gamma_j} u_{lmk}^{*}\left(\mathbf{y}_i, \mathbf{x}_j\right) n_m\left(\mathbf{y}_i\right) d\Gamma_j \right) p_k\left(\mathbf{x}_j\right) \quad \text{for } i = 1, 2, \ldots, M \end{aligned} \tag{A.13}$$

where $n_m\left(\mathbf{y}\right)$ is the normal unit-vector at $\mathbf{y}$ pointing into domain Ω from sub-domain Ω_y, as shown in Fig. A.1. The third-order tensors u_{lmk}^{*} and p_{lmk}^{*} that represent the fundamental solutions of the stress-state [24] can be given as closed-form expressions:

$$u_{lmk}^{*} = -\frac{1}{4\pi} \left[A\left(r_{,l}\delta_{mk} + r_{,m}\delta_{lk} - r_{,k}\delta_{lm} \right) + B r_{,l} r_{,m} r_{,k} \right] \tag{A.14}$$

$$\begin{aligned} p_{lmk}^{*} = \frac{\rho c_S^2}{4\pi} \Bigg[& - A\frac{2}{r}\left(n_l\delta_{mk} + n_m\delta_{lk}\right) + D\left(r_{,k}\delta_{lm}\frac{\partial r}{\partial n} + r_{,l} r_{,m} n_k \right) + \\ & E\left(\frac{\partial r}{\partial n}\left[r_{,l}\delta_{mk} + r_{,m}\delta_{lk} \right] + r_{,m} r_{,k} n_l + r_{,l} r_{,k} n_m \right) + \\ & F r_{,l} r_{,m} r_{,k}\frac{\partial r}{\partial n} + G n_k \delta_{lm} \Bigg] \end{aligned} \tag{A.15}$$

where

$$D = 2\left[\frac{d^2\psi}{dr^2} - \frac{1}{r}\left(\frac{d\psi}{dr} + \frac{d\chi}{dr}\right) + \frac{\chi}{r^2}\right] \tag{A.16}$$

$$E = -\frac{d^2\psi}{dr^2} + \frac{1}{r}\left(\frac{d\psi}{dr} + 3\frac{d\chi}{dr}\right) - 6\frac{\chi}{r^2} \tag{A.17}$$

$$F = 4\left[\frac{3}{2}\frac{d^2\chi}{dr^2} - \frac{5}{r}\frac{d\chi}{dr} + 7\frac{\chi}{r^2}\right] \tag{A.18}$$

$$G = -2\left(\frac{d^2\psi}{dr^2} + 2\frac{d^2\chi}{dr^2}\right) \tag{A.19}$$

and the other variables are the same as those defined in Eqs. (A.4)–(A.11).

Appendix B. Block-diagonal matrices

The block-diagonal matrices that contain the sub-matrices from each pile's displacement FRF matrix in the pile-group are:

$$\begin{aligned}
\mathbf{H}_{\mathrm{P11}} &= \begin{bmatrix} \mathbf{H}^1_{\mathrm{P11}} & \mathbf{0} & \dots & \mathbf{0} \\ \mathbf{0} & \mathbf{H}^2_{\mathrm{P11}} & & \mathbf{0} \\ \vdots & & \ddots & \vdots \\ \mathbf{0} & \mathbf{0} & \dots & \mathbf{H}^N_{\mathrm{P11}} \end{bmatrix}, \quad \mathbf{H}_{\mathrm{P12}} = \begin{bmatrix} \mathbf{H}^1_{\mathrm{P12}} & \mathbf{0} & \dots & \mathbf{0} \\ \mathbf{0} & \mathbf{H}^2_{\mathrm{P12}} & & \mathbf{0} \\ \vdots & & \ddots & \vdots \\ \mathbf{0} & \mathbf{0} & \dots & \mathbf{H}^N_{\mathrm{P12}} \end{bmatrix}, \\
\mathbf{H}_{\mathrm{P21}} &= \begin{bmatrix} \mathbf{H}^1_{\mathrm{P21}} & \mathbf{0} & \dots & \mathbf{0} \\ \mathbf{0} & \mathbf{H}^2_{\mathrm{P21}} & & \mathbf{0} \\ \vdots & & \ddots & \vdots \\ \mathbf{0} & \mathbf{0} & \dots & \mathbf{H}^N_{\mathrm{P21}} \end{bmatrix}, \quad \mathbf{H}_{\mathrm{P22}} = \begin{bmatrix} \mathbf{H}^1_{\mathrm{P22}} & \mathbf{0} & \dots & \mathbf{0} \\ \mathbf{0} & \mathbf{H}^2_{\mathrm{P22}} & & \mathbf{0} \\ \vdots & & \ddots & \vdots \\ \mathbf{0} & \mathbf{0} & \dots & \mathbf{H}^N_{\mathrm{P22}} \end{bmatrix}.
\end{aligned} \tag{B.1}$$

The block-diagonal transformation matrices that couple the field variables at the soil-pile interface to each pile's centroidal axis are:

$$\mathbf{Q}_1 = \begin{bmatrix} \mathbf{Q}_1^1 & \mathbf{0} & \dots & \mathbf{0} \\ \mathbf{0} & \mathbf{Q}_1^2 & & \mathbf{0} \\ \vdots & & \ddots & \vdots \\ \mathbf{0} & \mathbf{0} & \dots & \mathbf{Q}_1^N \end{bmatrix}, \ \mathbf{Q}_2 = \begin{bmatrix} \mathbf{Q}_2^1 & \mathbf{0} & \dots & \mathbf{0} \\ \mathbf{0} & \mathbf{Q}_2^2 & & \mathbf{0} \\ \vdots & & \ddots & \vdots \\ \mathbf{0} & \mathbf{0} & \dots & \mathbf{Q}_2^N \end{bmatrix}. \tag{B.2}$$